UCLA
UCLA Previously Published Works

Title
Super-enhancers promote transcriptional dysregulation in nasopharyngeal carcinoma

Permalink
https://escholarship.org/uc/item/4w9382nt

Journal
Cancer Research, 77(23)

ISSN
0008-5472

Authors
Yuan, Jiang
Jiang, Yan-Yi
Mayakonda, Anand
et al.

Publication Date
2017-12-01

DOI
10.1158/0008-5472.can-17-1143

Peer reviewed

eScholarship.org Powered by the California Digital Library
University of California

Author Manuscript

Author Manuscript

Author Manuscript

Author Manuscript

HHS Public Access

Author manuscript

Cancer Res. Author manuscript; available in PMC 2019 July 18.

Published in final edited form as:

Cancer Res. 2017 December 01; 77(23): 6614–6626. doi:10.1158/0008-5472.CAN-17-1143.

Super-Enhancers Promote Transcriptional Dysregulation in Nasopharyngeal Carcinoma

Jiang Yuan[#1], **Yan-Yi Jiang**[#1], **Anand Mayakonda**[1], **Moli Huang**[1], **Ling-Wen Ding**[1], **Han Lin**[1], **Fenggang Yu**[2], **Yanan Lu**[2], **Thomas Kwok Seng Loh**[2,3], **Marilynn Chow**[4], **Samantha Savage**[4], **Jeffrey W. Tyner**[4], **De-Chen Lin**[1,5], and **H. Phillip Koeffler**[1,5,6]

[1]Cancer Science Institute of Singapore, National University of Singapore, Singapore.

[2]Department of Otolaryngology, National University Hospital Singapore, Singapore.

[3]National University Cancer Institute of Singapore, National University Health System, Singapore.

[4]Department of Cell, Developmental & Cancer Biology, Knight Cancer Institute, Oregon Health & Science University, Portland, Oregon.

[5]Department of Medicine, Cedars-Sinai Medical Center, University of California, Los Angeles School of Medicine, Los Angeles, California.

[6]National University Cancer Institute, National University Hospital Singapore, Singapore.

[#] These authors contributed equally to this work.

Abstract

Nasopharyngeal carcinoma (NPC) is an invasive cancer with particularly high incidence in Southeast Asia and Southern China. The pathogenic mechanisms of NPC, particularly those involving epigenetic dysregulation, remain largely elusive, hampering clinical management of this malignancy. To identify novel druggable targets, we carried out an unbiased high-throughput chemical screening and observed that NPC cells were highly sensitive to inhibitors of cyclin-dependent kinases (CDK), especially THZ1, a covalent inhibitor of CDK7. THZ1 demonstrated

Corresponding Authors: Yan-Yi Jiang, National University of Singapore, 14 Medical Drive, #13 North Core, Singapore 117599, Singapore. Phone: 65-6516-2162; Fax: 65-6516-2162; csijy@nus.edu.sg; and De-Chen Lin, De-Chen.Lin@cshs.org.
J. Yuan and Y.-Y. Jiang contributed equally to this article.

Authors' Contributions

Conception and design: J. Yuan, Y.-Y. Jiang, D.-C. Lin

Development of methodology: D.-C. Lin

Acquisition of data (provided animals, acquired and managed patients, provided facilities, etc.): F. Yu, Y. Lu, T.K.S. Loh, J.W. Tyner

Analysis and interpretation of data (e.g., statistical analysis, biostatistics, computational analysis): J. Yuan, A. Mayakonda, M. Huang, D.-C. Lin

Writing, review, and/or revision of the manuscript: J. Yuan, J.W. Tyner, D.-C. Lin

Administrative, technical, or material support (i.e., reporting or organizing data, constructing databases): L.-W. Ding, M. Chow, S. Savage

Study supervision: D.-C. Lin, H.P. Koeffler

Disclosure of Potential Conflicts of Interest

J.W. Tyner reports receiving other commercial research support from Agios, Aptose, Array, AstraZeneca, Constellation, Genentech, Incyte, Janssen, Seattle Genetics, Syros, and Takeda and is a consultant/advisory board member for Leap Oncology. No potential conflicts of interest were disclosed by the other authors.

The costs of publication of this article were defrayed in part by the payment of page charges. This article must therefore be hereby marked *advertisement* in accordance with 18 U.S.C. Section 1734 solely to indicate this fact.

Note: Supplementary data for this article are available at Cancer Research Online (http://cancerres.aacrjournals.org/).

Author Manuscript Author Manuscript Author Manuscript Author Manuscript

pronounced antineoplastic activities both *in vitro* and *in vivo.* An integrative analysis using both whole-transcriptome sequencing and chromatin immunoprecipitation sequencing pinpointed oncogenic transcriptional amplification mediated by super-enhancers (SE) as a key mechanism underlying the vulnerability of NPC cells to THZ1 treatment. Further characterization of SE-mediated networks identified many novel SE-associated oncogenic transcripts, such as BCAR1, F3, LDLR, TBC1D2, and the long noncoding RNA TP53TG1. These transcripts were highly and specifically expressed in NPC and functionally promoted NPC malignant phenotypes. Moreover, DNA-binding motif analysis within the SE segments suggest that several transcription factors (including ETS2, MAFK, and TEAD1) may help establish and maintain SE activity across the genome. Taken together, our data establish the landscape of SE-associated oncogenic transcriptional network in NPC, which can be exploited for the development of more effective therapeutic regimens for this disease.

Introduction

Nasopharyngeal carcinoma (NPC) is a malignant tumor derived from the epithelial cells of the nasopharynx, with high prevalence in epidemic regions including Southern China, Southeast Asia, Northern Africa, and Alaska (1, 2). Such unique geographic and ethnic distribution likely reflects the multifactorial etiology of NPC, including genetic susceptibility, Epstein-Barr virus infection, heredity, and environmental influences, such as consumption of salt-preserved fish (3–5). We have previously profiled NPC genomic abnormalities and demonstrated a high degree of intertumor heterogeneity of NPC and infrequent targetable genetic lesions (6). Recent genomic analysis from others confirmed that genetic defects often disrupt tumor suppressor genes rather than druggable oncogenes (7, 8). Hence, alternative molecular approaches in addition to genomic profiling are required for the identification of novel drug candidates and understanding the pathophysiologic mechanisms of NPC.

Here, to discover therapeutic candidates and novel oncogenes in NPC, we performed an unbiased high-throughput chemical screen. We observed that NPC is particularly vulnerable to THZ1, which epigenetically blocks the transcriptional output from Pol II (9). As global epigenomic dysregulation in NPC has yet to be delineated, we proceeded to address this and found that the venerability of NPC cells to THZ1 was associated with the activation of super-enhancers (SE). SEs are large clusters of genomic regulatory elements that can be revealed by enhancer marks such as acetylation of histone H3 lysine 27 (H3K27ac) and mono-methylation of histone H3 at lysine 4 (H3K4me1; ref. 10). In differentiation cells, SEs are constantly associated with key lineage-specific genes that control cell identity. Moreover, in multiple types of cancer cells, SEs are enriched at oncogenes and other transcripts important for tumor pathogenesis. Indeed, we and others have shown that SEs drive oncogene expression through efficiently recruiting the transcriptional apparatus (11–16).

SEs have not been characterized in NPC, and whether and how they play a role in NPC biology remains unknown. To this end, we established the SE landscape in NPC cells and found that SE-associated genes, but not typical enhancer (TE)–associated genes, showed exceptional sensitivity to THZ1 treatment. Further investigations unveiled a number of novel

Author Manuscript Author Manuscript Author Manuscript Author Manuscript

SE-associated oncogenic transcripts, as well as master transcription factors (TF) that help activate and maintain SEs.

Materials and Methods

NPC cell lines

NPC cell line HK1 was kindly provided by Dr. Goh Boon Cher (Cancer Science Institute of Singapore, Singapore). S18, S26, SUNE1, and SUNE2 cells were generously given by Dr. Mu-Shen Zeng (Sun Yat-sen University Cancer Center, Guangzhou, China). HNE1 cells were purchased from NPC AoE Research Tissue Bank and Cell Line Repository. C666-1 and SUNE1 cell lines were cultured in RPMI1640 medium; HK1, SUNE2, S18, S26, HNE1, and HEK293T were maintained in DMEM. All media were supplemented with 10% FBS (HyClone), penicillin (100 U/mL), and streptomycin (100 mg/mL), respectively. Cells were grown at 37°C and 5% CO_2.

Primary nonmalignant human nasopharyngeal cells

We derived primary nonmalignant human nasopharyngeal cells (PNHNC) using an established protocol (17). Briefly, nonmalignant nasopharyngeal epithelium was washed extensively in Hank's balanced salt solution, digested in 10 mg/mL of dispase II, and dissociated by repetitive pipetting. The dissociated cells were finally washed twice and were ready for culturing as monolayer cells.

IHC analysis

Human NPC tissue microarrays contained paraffin-embedded tumors and the adjacent normal. IHC analysis was performed as described previously (18). The samples were incubated with antibodies against BCAR1 (Abcam; ab80016), ETS2 (GeneTex; GTX104527), F3 (Novus Biologicals; TF9–10H10), LDLR (Abcam; ab52818), and TBC1D2 (Novus Biologicals; NBP1–87335) overnight at 4°C. Immunostaining was performed using the PV-9000 Polymer Detection System with diaminobenzidine (DAB) according to the manufacturer's recommendations (GBI). Staining intensity was graded on the scales: 0 (negative), 1 (weak), 2 (moderate) as low expression and 3 (strong) as high expression.

Construction and infection of shRNA-expressing lentivirus

The pLKO.1-CDK7 and ETS2-shRNA were generated by inserting double-stranded oligonucleotides into pLKO.1-puro lentiviral vector and were confirmed by DNA sequencing. Recombinant lentiviral vectors and packaging vectors (pCMV-dR8.91 and pMD2.G-VSVG) were cotransfected into 293T cells using Lipofectamine 2000 according to the manufacturer's instructions. Supernatants containing lentiviralexpressing shRNA were harvested 48 hours after transfection; NPC cells were infected with the lentiviruses in the presence of 8 mg/mL Polybrene (Sigma-Aldrich).

Author Manuscript Author Manuscript Author Manuscript Author Manuscript

High-throughput small-molecule inhibitor screening

High-throughput small-molecule inhibitor screening was implemented as described previously (13). Using a semiautomated platform, we tested 126 small-molecule compounds against seven NPC cell lines. Briefly, 250 cells were seeded in each well of a 384-well plate and treated with a gradient concentration of individual compounds in an 8-point, 3-fold dilution fashion (including control). Three days later, cell viability was evaluated in each well using a tetrazolium-based MTS assay. The absorbance values from the MTS assay were normalized to the average of 48 wells per plate containing no-drug control, and these normalized values were used to fit a third-order polynomial curve to determine the dose response of each drug. Mean inhibitory concentration (IC_{50}) was calculated using nonlinear regression analysis in GraphPad Prism 6.0.

Antibodies and chemicals

Antibodies—The following antibodies were used: CDK7 (Cell Signaling Technology; 2916); RNAPII CTD S2 (Bethyl Laboratories; A300–654A), RNAPII CTD S5 (Bethyl Laboratories; A300–655A), RNAPII CTD S7 (Cell Signaling Technology; 13780), RNAPII (Santa Cruz Biotechnology; sc-899), BCAR1 (Abcam; ab80016), ETS2 (GeneTex; GTX104527 and Santa Cruz Biotechnology; sc-365666X), F3 (Novus Biologicals; TF9–10H10), LDLR (Abcam; ab52818), TBC1D2 (Novus Biologicals; NBP1–87335), GAPDH (Abcam; ab46540), anti-rabbit IgG (Cell Signaling Technology; 7074), H3K27ac (Abcam; ab4729), H3K4me1 (Abcam; ab8895), H3K4me3 (Abcam; ab8580), and RNA Pol II (Santa Cruz Biotechnology; sc-899 X).

Chemicals—AT7519 (S1524), flavopiridol (S1230), JNJ-7706621 (S1249), LEE011 (S7440), roscovitine (S1153), and SNS-032 (S1145) were obtained from Selleckchem. AZD-5438 (A8326), CDK4 inhibitor (B1233), CDK9 inhibitor (A3294), CVT-313 (A3336), LDC000067 (B4754), purvalanol B (A8565), palbociclib (A8316), and THZ1 (A8882) were purchased from ApexBio.

RNA extraction, cDNA synthesis, and quantitative RT-PCR

Total RNA was extracted by RNeasy Mini Kit (Qiagen), and cDNA was synthesized using iScript cDNA Synthesis Kit (Applied Biosystems) according to the manufacturer's instructions. qRT-PCR was conducted with PrecisionFAST Master Mix (Precision, Precision-LR). Expression values were normalized by GAPDH and expressed as relative to those of control samples.

Mice xenograft and tumor metastasis assay

All murine studies were performed under the ethical regulations of the Institutional Animal Care and Use Committee of National University of Singapore (Singapore). Briefly, 1×10^6 NPC C666-1 cells were injected subcutaneously into each flank of recipient NOD/SCID gamma (NSG) mice (6 weeks old, 10 mice). Tumors were allowed to grow for 15 days, after which the mice were randomized into two groups and treated with either vehicle or THZ1 via intraperitoneal injection (10 mg/kg, twice daily). Body weight, tumor growth, and general behavior of the mice were monitored. Tumor sizes were measured every 4 days for a

Author Manuscript Author Manuscript Author Manuscript Author Manuscript

total of 4 weeks. At the end of the experiment, mice were euthanized, and tumors were surgically dissected, weighed, and analyzed.

NPC C666-1 cells (1×10^6) were injected into adult NSG mice via tail vein (6 weeks old, 14 mice). When the grafted cells metastasized into lungs (about 45 days), mice were randomly divided into two groups and treated with either vehicle or THZ1 (10 mg/kg, twice daily). After 4 weeks of treatment, mice were euthanized; lungs were removed and fixed in Bouin's solution. Number of lung nodules were counted and embedded in paraffin. hematoxylin and eosin and IHC staining were performed on 5-μm sections of paraffin-embedded tumors.

RNA sequencing and data analysis

RNA sequencing (RNA-seq) was performed as described previously (19). Briefly, sequencing libraries were prepared using TruSeq RNA Library Prep Kit (Illumina) according to the manufacturer's protocol and were sequenced on HiSeq 2000 sequencer (Illumina). Paired-end reads (100 bp) were aligned to hg19 reference genome with Ensembl gtf (version 75) provided as a known junction file, using splice-aware STAR aligner. Expression level was measured as FPKM using Stringtie software against Ensembl v75 gtf.

Chromatin immunoprecipitation, sequencing, and analysis

Chromatin immunoprecipitation (ChIP) with antibodies H3K27ac (Abcam; ab4729), H3K4me1 (Abcam; ab8895), H3K4me3 (Abcam; ab8580), and RNA Pol II (Santa Cruz Biotechnology; sc-899 X) was performed as described previously (13). Briefly, NPC cells were crosslinked and sonicated to obtain chromatin DNA fragments between 200 and 250 bp with a Bioruptor Sonicator (Diagenode). Sonicated lysates were cleared and incubated with magnetic beads bound with antibodies. ChIP DNA was eluted, reverse crosslinked, precipitated, and sequenced on Illumina HiSeq 2000.

Single-end 50-bp reads were aligned to hg19 reference genome using Bowtie aligner with parameter -m2-k 2 -best -strata −1 49. MACS2 was used for peak calling with parameter -B -SPMR -no-model -ext-size 200 -q 0.01. MACS argument -broad was used for all histone ChIP sequencing (ChIP-seq). Duplicate reads were not considered for peak calling. ChIP-seq heatmaps were drawn using deepTools plotHeatmap function. Pileup signal (bedgraph files) generated by MACS2 were converted to big-wig files using bed-GraphToBigWig and visualized in IGV.

SEs were identified using ROSE by stitching peaks within a 12-kb interval. Stitched enhancers were classified as SEs or TEs and assigned to the nearest ensemble genes.

Assay for transposase-accessible chromatin with high-throughput sequencing and data analysis

Assay for transposase-accessible chromatin with high-throughput sequencing (ATAC-seq) was performed using the published protocol (20). ATAC-seq data were analyzed similar to ChIP-seq but with the following exceptions: Reads were trimmed by 15 bp in $5' \rightarrow 3'$ with Bowtie argument -trim5 15 during alignment. Reads mapped to mitochondrial DNA were removed.

Author Manuscript Author Manuscript Author Manuscript Author Manuscript

Motif analysis

DNA segments constituting SEs were extracted and used for motif analysis by Homer (http://homer.ucsd.edu/homer/motif/). Homer script findMotifsGenome.pl was run on all SE constituent segments with argument “hg19 -size 200 -len 10 -noMotif” to detect enrichment of known TF motifs. Homer results were further manually analyzed, and those motifs with high background enrichment were removed.

Gene Ontology and gene set enrichment analysis

Gene Ontology (GO) was performed using ConsensusPathDB (ConsensusPathDB.org). Significantly enriched biological processes were defined as $P < 0.01$. Gene set enrichment analysis (GSEA) for SE and TE was performed as described previously (13).

Results

Prominent sensitivity of NPC cells to CDK7 inhibition

To identify druggable candidates in NPC pathogenesis, we carried out an unbiased high-throughput screen with a library of 126 small-molecule compounds targeting prosurvival kinases and nonkinase oncoproteins (21, 22). Seven NPC cell lines were tested in the screening, and a cell viability assay was employed to measure their sensitivity to each compound (Fig. 1A; Supplementary Table S1). A total of 12 compounds exhibited antiproliferation effects with a mean IC_{50} of less than 600 nmol/L across all seven NPC cell lines (Fig. 1A; Supplementary Table S1). These consisted of known anti-NPC inhibitors, including chemicals targeting the HSP family (23), PI3K/AKT/MTOR (24), and RTK (Supplementary Fig. S1; ref. 25).

Among them, NPC cell lines showed pronounced sensitivity to CDK inhibitors (Fig. 1A; Supplementary Fig. S1). As different CDK inhibitors elicit distinct cellular responses through targeting either different cell-cycle or transcriptional regulators (26, 27), we further investigated them using 14 different CDK inhibitors in seven NPC cell lines. Only four of these 14 CDK inhibitors suppressed NPC proliferation at nanomolar concentrations (Supplementary Table S2). Interestingly, among them, THZ1, SNS032, and flavopiridol share only one target, CDK7 (Fig. 1B; Supplementary Table S2). We and others have recently reported that THZ1 decreased cell viability in multiple types of cancers via suppressing CDK7-dependent transcription activation (9, 13–16). However, the biological significance of CDK7 inhibition in NPC cells remains unknown; thus, we next explored this question.

THZ1 significantly inhibits NPC cell growth both *in vitro* and *in vivo*

We first investigated the growth-inhibitory effects of CDK7 inhibition in NPC C666-1 and HK1 cells, as they were the most sensitive cell lines upon THZ1 treatment (Fig. 1C). Depletion of CDK7 with lentiviral-based shRNAs confirmed that CDK7 is required for both the proliferation and survival of NPC cells (Fig. 1D; Supplementary Fig. S2). Consistently, NPC cells treated with THZ1 underwent marked growth retardation and cell-cycle arrest in G_2-M stage (Fig. 1E; Supplementary Figs. S3 and S4). Moreover, THZ1 profoundly induced

Author Manuscript Author Manuscript Author Manuscript Author Manuscript

cell apoptosis (Fig. 1F). Importantly, THZ1 failed to elicit such effects in PNHNC cells (Supplementary Fig. S5), strongly suggesting the tumor-specific effect of THZ1.

We next tested the antitumor effects of THZ1 in NSG murine models. C666-1 NPC cells were inoculated either subcutaneously or through the tail vein for assaying xenograft growth and metastasis potential, respectively. Mice bearing tumors were randomized into two groups and treated with either vehicle or THZ1 twice daily (10 mg/kg). THZ1 displayed a striking tumor-suppressive function, such that the xenograft barely proliferated in the treatment group (Fig. 2A; Supplementary Fig. S6A and S6B). IHC analysis of tumor sections confirmed markedly decreased proliferation and increased apoptosis in the THZ1 treatment group, as indicated by Ki67 and cleaved caspase-3 (CC3) staining, respectively (Fig. 2B).

THZ1 also significantly inhibited NPC cell metastasis, resulting in a remarkable reduction of the number of metastatic lesions in the lungs (Fig. 2C; Supplementary Fig. S6C). Of note, we did not observe significant loss of body weight (Supplementary Fig. S6D) or other common toxic effects (e.g., diarrhea, rash, etc.; data not shown) in mice treated with THZ1.

To further determine whether the effect of THZ1 was through either inhibition of angiogenesis or direct suppression of the proliferation of NPC cells, we performed additional xenograft assays, in which the xenografts were allowed to grow until 20 mm^3 before the administration of THZ1. In this experimental setting, THZ1 again exhibited prominent anti-NPC activity (Supplementary Fig. S7A and S7B). Furthermore, IHC for CD31 staining indicated that the antineoplastic property of THZ1 was a result of direct inhibition of tumor proliferation rather than reduction of angiogenesis (Supplementary Fig. S7C). Taken together, these data strongly suggest that THZ1 exhibited high potency against the viability of NPC cells both *in vitro* and *in vivo.*

THZ1 treatment suppresses general and selective transcription in NPC cells

We next probed the molecular mechanisms underlying the antineoplastic function of THZ1 in NPC. Studies have shown that CDK7 regulates the activity of RNA polymerase II (Pol II) through phosphorylating its carboxy-terminal domain (CTD), thus promoting the transition from transcriptional initiation to elongation (28–30). Indeed, as a covalent inhibitor of CDK7, THZ1 decreased Pol II CTD phosphorylation at serines 2, 5, and 7 in a dose- and time-dependent manner in NPC cells (Fig. 2D; Supplementary Fig. S8).

We next performed whole-transcriptome sequencing (RNA-seq) to compare the global gene abundance in C666-1, HK1, and HNE1 cells following exposure to either THZ1 (200 nmol/L) or DMSO for 6 hours. Results showed that a group of transcripts were quickly downregulated in a selective fashion upon treatment with low concentration of THZ1 (Fig. 2E; Supplementary Table S3). A considerable proportion of transcripts were upregulated, which was possibly because they are either Pol II independent, induced by negative feedback or other cellular stresses. GO analysis revealed that these THZ1-sensitive transcripts were significantly enriched in processes related to transcriptional regulation, DNA damage repair, and cell cycle (Fig. 2F), suggesting that these transcripts likely mediate the exceptional antineoplastic property of THZ1.

Author Manuscript Author Manuscript Author Manuscript Author Manuscript

We next characterized further the biological features of these THZ1-sensitive transcripts in NPC cells. As has been shown by our group (13) and others (9, 14–16), SE-associated mRNAs were hypersensitive to transcriptional blockade, and in several types of cancers, they were significantly enriched in those transcripts remarkably vulnerable to THZ1 treatment. As the SE landscape of NPC cells has not been established, we proceeded to address this question.

The landscape of SEs in NPC

We generated the SE landscape in three NPC cell lines through ChIP-seq using H3K27ac antibody as described previously (13). To establish comprehensive active enhancer and promoter catalogs, we further performed ChIP-seq with antibodies against H3K4me3, H3K4me1, as well as Pol II.

A total of 1,098, 796, and 868 SE-associated transcripts were identified in C666-1, HK1, and HNE1 cells, respectively (Fig. 3A; Supplementary Fig. S9; Supplementary Tables S4 and S5). Not surprisingly, a number of well-defined NPC oncogenes were associated with SEs, such as *MYC* (31, 32), *TP63* (33, 34), and *EGFR* (35, 36). Several known oncogenic long noncoding RNAs (LncRNA), such as *MALAT1, NEAT1,* and *CCAT1,* were also associated with SEs in NPC (Fig. 3A; refs. 37–39). Notably, H3K27ac modification was much weaker in these oncogenes (e.g., EGFR and MALAT1) in PNHNC cells (Supplementary Fig. S9). H3K27ac signals showed consensus profiles among the three NPC cell lines (Fig. 3B and C). In addition, highly concordant occupancy of H3K4me3 and H3K4me1 peaks with H3K27ac validated the robustness of our SE profiling approach (Fig. 3C and D).

To further corroborate the NPC SE profiles, we employed a recently developed assay, ATAC-seq, to define accessible chromatin regions (Supplementary Table S6). Indeed, ATAC-Seq peaks overlapped significantly with H3K27ac, H3K4me3, and H3K4me1 signals, further confirming the active chromatin regions that we have identified in NPC cells (Fig. 3C and D).

As SE drives expression of oncogenes to promote the malignant phenotype of multiple cancer types (9, 13–16), GO analysis was performed to explore the functional implications of these SE-associated transcripts in NPC cells. Importantly, SE-associated genes were significantly enriched in the processes controlling “Cancer Hallmarks,” such as the regulation of cell proliferation, apoptosis, migration, and RNAPII-mediated transcription (Fig. 3E). However, such enrichment was not noted in PNHNC cells (Supplementary Fig. S10).

Biological features of SE-associated transcripts

To further characterize the biological features of SE-associated transcripts in NPC, the expression level of SE-associated transcripts was first examined using our RNA-seq data from the same three NPC cell lines. RNA abundance of SE-associated transcripts was significantly higher compared with that of TE-associated transcripts (Fig. 4A). Moreover, the RNA level of SE-associated transcripts was significantly downregulated upon THZ1 treatment, compared with TE-associated transcripts (Fig. 4B). In addition, GSEA showed

Author Manuscript Author Manuscript Author Manuscript Author Manuscript

that SE-associated transcripts were preferentially enriched for those genes that were sensitive to THZ1 treatment (Fig. 4C) relative to TE-associated transcripts.

Next, ChIP-seq analysis was performed using Pol II antibody in the presence and absence of THZ1, which confirmed that THZ1 treatment led to a strong reduction in Pol II binding at the promoters of SE-associated genes in a genome-wide fashion. In contrast, the decrease of binding was only moderate in TE-associated genes (Fig. 4D).These results were consistent across all three NPC cell lines and suggested that SE-associated genes were disproportionally sensitive to CDK7 inhibition in NPC cells.

We also observed many genes that were uniquely expressed in NPC cells using the dataset containing RNA-seq results from 675 human cancer cell lines (Fig. 4E; Supplementary Table S7), supporting the notion that SEs orchestrate a lineage-specific expression pattern helping to control cell identity (40).

Integrative analysis identifies novel candidate oncogenic transcripts

To identify novel candidate oncogenes associated with SEs in NPC, an integrative analysis of the dynamics of both RNA-seq and ChIP-seq was implemented. We and others have found that SE-driven oncogenes often exhibit high expression in cancer and had increased sensitivity to transcription inhibition compared with TE-associated genes. We selected candidate SE-associated oncogenes by requiring that their mRNA abundances were: (i) within the top 15% of all expressed transcripts in NPC cells and (ii) rapidly downregulated by THZ1 treatment. This integrative analysis generated a list of genes, including many well-established oncogenes such as *EGFR, MYC, MCL1,* and *FSCN1,* underscoring the effectiveness of our approach to identify bona fide oncogenic candidates. Importantly, the list also included a total of 15 candidate transcripts not previously implicated in NPC biology (Fig. 5A).

Their biological relevance was next investigated. A focused functional screen in HK1 cells was performed by knocking down each of the 15 candidates with siRNA, and carrying out cell viability and colony formation assay (Supplementary Fig. S11A; Supplementary Table S8). As a result, we identified four genes, *BCAR1, F3, FDFR, TBC1D2,* whose depletion led to significant reduction of both cell viability and clonogenic capacity of HK1 cells (Fig. 5B and C; Supplementary Fig. S11B and S11C). Their pronounced sensitivity to THZ1 treatment was confirmed at both the mRNA and protein levels (Fig. 5D; Supplementary Fig. S11D and S11E). Importantly, depletion of these genes had no significant effect on the proliferation of PNHNC cells (Supplementary Fig. S12). In sharp contrast, the RNA and protein products of TE-associated genes were either only modestly decreased or remained unaltered upon exposure to THZ1 (Supplementary Fig. S13).

Following the initial screen in HK1 cells, we extended the functional experiments to other NPC lines. Specifically, we measured the expression level of these four candidate genes in seven NPC lines, and additional cells with high expression of these proteins were selected for colony formation assay. Importantly, silencing each of these four oncogenes significantly impaired cell viability and clonogenic capacity in at least two of seven NPC lines (Fig. 5E). Moreover, to evaluate their protein expression in NPC tissue, we performed IHC staining

Author Manuscript Author Manuscript Author Manuscript Author Manuscript

and confirmed that all four candidate oncogenes exhibited strong expression in primary NPC tissues; in contrast, their protein levels were either low or undetectable in adjacent nonmalignant tissues (Fig. 5F).

In addition to coding transcripts, SE-associated LncRNAs in NPC were explored. According to RNA-seq and ChIP-seq databases, we selected six candidate novel LncRNAs showing the highest expression in NPC cell lines: MIR205HG, LINC00152, NEAT1, LINC00941, TP53TG1, and MALAT1. Both *NEAT1* and *MALAT1* are known oncogenic LncRNAs overexpressed in many types of cancers, supporting the usefulness of this approach to nominate genuine oncogenic transcripts (41, 42). Concerning the other four LncRNAs, they have not been characterized in detail in human cancers, prompting the investigation of their functional implication in NPC cells. Of note, among the four candidate LncRNAs, silencing of TP53TG1 led to decreased cell proliferation and colony-forming ability in three NPC cell lines that had high expression of this LncRNA (Fig. 5G; Supplementary Fig. S14). In contrast, no effect on the proliferation of PNHNC cells was noted upon TP53TG1 knockdown (Supplementary Fig. S12).

We next performed a series of gain-of-function experiments to explore whether these candidate genes might regulate the sensitivity of NPC cells to THZ1 treatment. Their ectopic expressions were confirmed by immunoblotting assay, and qPCR analysis, colony formation, and cell proliferation assay demonstrated that none of these candidate genes was capable of alleviating the cell toxicity elicited by THZ1 (Supplementary Fig. S15).

Characterization of SE-promoting TFs in NPC

Recent studies in a few cell types (e.g., murine embryonic stem cells) have suggested that a small set of the many hundreds of TFs (core TFs) contributes to the establishment and maintenance of SEs global, thus controlling the gene expression programs that are involved in cell fate determination and lineage-specific differentiation (43). These TFs are found to be highly (and often lineage specifically) expressed in their corresponding cell types and are usually associated with SEs themselves, forming autoregulatory loops. To gain insights into the TFs involved in SE-associated transcriptional regulation of NPC cells, *de novo* DNA-binding motif analysis was performed within SE (Fig. 6A; Supplementary Tables S9–S11). A total of 62, 47, and 66 DNA-binding motifs were significantly enriched in SE segments compared with genome background in C666-1, HK1, and HNE1 cells, respectively. Next, three TFs (MAFK, ETS2, and TEAD1) were further studied after requiring that: (i) each was associated with SE itself, (ii) their motifs and expression could be detected in all three cell lines (Fig. 6B; Supplementary Fig. S16). We reasoned that, as SE-associated transcriptional activation was necessary for sustaining NPC cell viability as shown by our earlier results, TFs that promote these SE-mediated transcriptions would be similarly required for cell proliferation. Therefore, knockdown assays were performed to examine the progrowth effect of these three TFs. Both TEAD1 and ETS2 robustly enhanced NPC cell proliferation and colony formation; in contrast, the PNHNC cells did not have increased proliferation with forced expression of TFs (Fig. 6C; Supplementary Fig. S12). We further confirmed that SE-associated TFs were extremely sensitive to THZ1 treatment (Fig. 6D).

Author Manuscript Author Manuscript Author Manuscript Author Manuscript

ETS2 is a novel SE-promoting TF

As ETS2 exhibited a more prominent role in supporting NPC cell growth than TEAD1 (Fig. 6C), the function of this TF was more closely explored (Fig. 6E). The progrowth effect of ETS2 was confirmed by two independent shRNAs both *in vitro* and *in vivo* (Fig. 7A and B), which was evident in multiple NPC cell lines having high ETS2 expression (Fig. 7C). IHC staining revealed that ETS2 protein level was significantly higher in primary NPC tissue compared with nonmalignant mucosa (Fig. 7D).

To determine how ETS2 regulates the global transcriptional program, RNA-seq was performed in ETS2-silenced cells. Two independent shRNAs produced highly similar results (Fig. 7E; Supplementary Table S12). GO analysis showed that downregulated genes upon loss of ETS2 were significantly involved in key processes for cancer biology, such as transcriptional regulation, cell death, and cell proliferation (Fig. 7F), reminiscent of SE-regulated processes (Fig. 3E). Importantly, downregulated genes contained a number of well-established oncogenes, such as FOS, MYC, SREBF1, etc. (Supplementary Fig. S17A), although the five candidate genes were not significantly altered by ETS2 depletion (Supplementary Fig. S17B). Meanwhile, GSEA analysis demonstrated that compared with TE-associated transcripts, SE-associated ones were preferentially enriched for genes that were decreased following ETS2 silencing (Fig. 7G; $P < 0.01$).

Discussion

Recent efforts in large-scale NPC genome analysis revealed extensive intertumor heterogeneity and scarce actionable mutant driver genes (6–8). With the aim of searching for alternative therapeutic strategies, we performed an unbiased high-throughput chemical screen in NPC cells and showed that they were highly sensitive to THZ1 treatment. As a CDK7 covalent inhibitor, THZ1 displayed potent anti-NPC effects both *in vitro* and *in vivo*, with minimum cytotoxicity in healthy mouse tissues.

To elucidate the acute sensitivity of NPC cells to THZ1 treatment, an integrative approach of both RNA-seq and ChIP-seq was performed to explore the dynamic changes in the activity of *cis*-regulatory regions across the genome. Notably, for all active genes upon THZ1 treatment, GSEA showed that genes in the leading edge were enriched in SE-associated transcripts, and these were most sensitive to THZ1 exposure (Fig. 5D). Moreover, the abundance of SE-associated transcripts was downregulated to a much greater degree by THZ1 compared with those associated with TEs (Supplementary Fig. S13). Together, these results suggest that SE-associated transcripts are particularly vulnerable to transcriptional blockade and that the SE-mediated transcriptional network at least partially accounts for the exceptional antineoplastic effects of THZ1 in NPC.

Another important result generated by our integrative analysis was the discovery of oncogenic transcripts in NPC. By considering (i) SE features, (ii) sensitivity to transcription inhibition, and (iii) RNA abundance, we nominated a list of genes, with many being established oncogenes in NPC and/or other cancer types. Importantly, this list also contained 19 candidate transcripts whose roles are unknown in NPC biology. Through extensive *in vitro* and *in vivo* functional analysis, we confirmed that five of these 19 SE-associated

Author Manuscript Author Manuscript Author Manuscript Author Manuscript

candidates (BCAR1, F3, LDLR, TBC1D2, and TP53TG1) contributed to cell survival and proliferation of NPC. Our IHC results further validated that these genes were highly expressed in primary NPC tissues, but not in adjacent normal tissue. Of note, the current work tested only the growth- and survival-related functions of putative oncogenes; candidate genes involved in other cellular processes (e.g., migration, invasion, and epithelial-mesenchymal transition) were not identified. Furthermore, this gene list was generated on the basis of three NPC cell lines, and further studies using primary NPC tissues are expected to uncover more NPC oncogenes.

Our analysis also validated its capability to discover important SE-associated LncRNAs. Not only did we find well-known oncogenic LncRNAs *(MALAT1* and *NEAT1)* in NPC, but a novel one, *TP53TG1,* was also identified and validated as an oncogenic LncRNA in NPC. TP53TG1 was originally isolated from a colon cancer cell line and observed to be induced by TP53 in response to cellular stress (e.g., ultraviolet irradiation and cisplatin exposure), indicating that TP53TG1 may be involved in the TP53 pathway in response to DNA damage (44). Very recently, Angel and colleagues reported that TP53TG1 might function as a tumor suppressor in colon and gastric cancer cells (45). In contrast, the current data support that TP53TG1 is associated with SE and promotes cell proliferation of NPC cells. These results suggest that the cancer-associated role of TP53TG1 may be context dependent, and future work is required to delineate its functions.

To explore in greater detail whether and how TFs are involved in promoting the activity of SE, we performed DNA-binding motif analysis and noted ETS2 as a novel SE-promoting TF in NPC. ETS2 (V-ets avian erythroblastosis virus E26 oncogene homolog 2) belongs to the ETS TF family and regulates genes involved in developmental processes by binding to the GGA(A/T) ETS response elements (46). In the context of cancer biology, ETS2 has seemingly opposite roles as it promoted telomerase activity and cancer progression in breast cancer (47) and glioblastoma multiforme (48), whereas the TFs suppressed tumor cell proliferation in non-small cell lung cancer (49). Interestingly, the stepwise development of NPC is associated with elevated level of ETS2 (50), in agreement with our current findings. Importantly, our GSEA analysis showed that genes downregulated following ETS2 knockdown were significantly enriched with SE-associated genes compared with TE-associated ones (Fig. 7G). Furthermore, ETS2-regulated gene expression signatures were similar to SE-regulated ones (Fig. 7F). Together, these results suggested that ETS2 may be a critical SE-promoting TF during NPC tumorigenesis.

In aggregate, the current study provides significant insights into SE-mediated transcriptional dysregulation in NPC cells, along with the identification of a number of novel SE-associated oncogenes. More importantly, our data suggest the potential therapeutic merit of blocking SE-associated oncogenic transcription for the treatment of this cancer.

Supplementary Material

Refer to Web version on PubMed Central for supplementary material.

Author Manuscript Author Manuscript Author Manuscript Author Manuscript

Acknowledgments

Grant Support

This research is supported by the National Research Foundation Singapore under its Singapore Translational Research Investigator Award (NMRC/STaR/0021/2014 to H.P. Koeffler) and administered by the Singapore Ministry of Health's National Medical Research Council (NMRC), the NMRC Centre Grant awarded to National University Cancer Institute of Singapore, the National Research Foundation Singapore, and the Singapore Ministry of Education under its Research Centres of Excellence initiatives (to H.P. Koeffler). D.-C. Lin was supported by the National Center for Advancing Translational Sciences UCLA CTSI Grant UL1TR000124 and the Tower Cancer Research Foundation. This study was also supported by the RNA Biology Center at the Cancer Science Institute of Singapore, NUS, as part of funding under the Singapore Ministry of Education's Tier 3 grants (grant no. MOE2014-T3-1-006 to H.P. Koeffler), the NCIS Yong Siew Yoon Research Grant through donations from the Yong Loo Lin Trust (to H.P. Koeffler), and the Terry Fox Foundation International Run Program through funds raised by the Terry Fox Singapore Run to National University Cancer Institute Singapore (NCIS; to H.P. Koeffler).

References

1. Wei WI, Sham JS. Nasopharyngeal carcinoma. Lancet 2005;365:2041–54. [PubMed: 15950718]
2. McDermott AL, Dutt SN, Watkinson JC. The aetiology of nasopharyngeal carcinoma. Clin Otolaryngol Allied Sci 2001;26:82–92. [PubMed: 11309046]
3. Bei JX, Li Y, Jia WH, Feng BJ, Zhou G, Chen LZ, et al. A genome-wide association study of nasopharyngeal carcinoma identifies three new susceptibility loci. Nat Genet 2010;42:599–603. [PubMed: 20512145]
4. Feng BJ, Huang W, Shugart YY, Lee MK, Zhang F, Xia JC, et al. Genome-wide scan for familial nasopharyngeal carcinoma reveals evidence of linkage to chromosome 4. Nat Genet 2002;31:395–9. [PubMed: 12118254]
5. Armstrong RW, Imrey PB, Lye MS, Armstrong MJ, Yu MC, Sani S. Nasopharyngeal carcinoma in Malaysian Chinese: salted fish and other dietary exposures. Int J Cancer 1998;77:228–35. [PubMed: 9650558]
6. Lin DC, Meng X, Hazawa M, Nagata Y, Varela AM, Xu L, et al. The genomic landscape of nasopharyngeal carcinoma. Nat Genet 2014;46:866–71. [PubMed: 24952746]
7. Zheng H, Dai W, Cheung AK, Ko JM, Kan R, Wong BW, et al. Whole-exome sequencing identifies multiple loss-of-function mutations of NF-kappaB pathway regulators in nasopharyngeal carcinoma. Proc Natl Acad Sci U S A 2016;113:11283–8. [PubMed: 27647909]
8. Li YY, Chung GT, Lui VW, To KF, Ma BB, Chow C, et al. Exome and genome sequencing of nasopharynx cancer identifies NF-kappaB pathway activating mutations. Nat Commun 2017;8:14121. [PubMed: 28098136]
9. Kwiatkowski N, Zhang T, Rahl PB, Abraham BJ, Reddy J, Ficarro SB, et al. Targeting transcription regulation in cancer with a covalent CDK7 inhibitor. Nature 2014;511:616–20. [PubMed: 25043025]
10. Heinz S, Romanoski CE, Benner C, Glass CK. The selection and function of cell type-specific enhancers. Nat Rev Mol Cell Biol 2015;16:144–54. [PubMed: 25650801]
11. Loven J, Hoke HA, Lin CY, Lau A, Orlando DA, Vakoc CR, et al. Selective inhibition of tumor oncogenes by disruption of super-enhancers. Cell 2013;153:320–34. [PubMed: 23582323]
12. Mansour MR, Abraham BJ, Anders L, Berezovskaya A, Gutierrez A, Durbin AD, et al. Oncogene regulation. An oncogenic super-enhancer formed through somatic mutation of a noncoding intergenic element. Science 2014;346:1373–7. [PubMed: 25394790]
13. Jiang YY, Lin DC, Mayakonda A, Hazawa M, Ding LW, Chien WW, et al. Targeting super-enhancer-associated oncogenes in oesophageal squamous cell carcinoma. Gut 2017;66:1358–68. [PubMed: 27196599]
14. Chipumuro E, Marco E, Christensen CL, Kwiatkowski N, Zhang T, Hatheway CM, et al. CDK7 inhibition suppresses super-enhancer-linked oncogenic transcription in MYCN-driven cancer. Cell 2014;159:1126–39. [PubMed: 25416950]

Author Manuscript Author Manuscript Author Manuscript Author Manuscript

15. Christensen CL, Kwiatkowski N, Abraham BJ, Carretero J, Al-Shahrour F, Zhang T, et al. Targeting transcriptional addictions in small cell lung cancer with a covalent CDK7 inhibitor. Cancer Cell 2014;26:909–22. [PubMed: 25490451]
16. Wang Y, Zhang T, Kwiatkowski N, Abraham BJ, Lee TI, Xie S, et al. CDK7-dependent transcriptional addiction in triple-negative breast cancer. Cell 2015;163:174–86. [PubMed: 26406377]
17. Liu X, Krawczyk E, Suprynowicz FA, Palechor-Ceron N, Yuan H, Dakic A, et al. Conditional reprogramming and long-term expansion of normal and tumor cells from human biospecimens. Nat Protoc 2017; 12:439–51. [PubMed: 28125105]
18. Jiang YY, Shang L, Shi ZZ, Zhang TT, Ma S, Lu CC, et al. Microtubule-associated protein 4 is an important regulator of cell invasion/migration and a potential therapeutic target in esophageal squamous cell carcinoma. Oncogene 2016;35:4846–56. [PubMed: 26876215]
19. Lin DC, Hao JJ, Nagata Y, Xu L, Shang L, Meng X, et al. Genomic and molecular characterization of esophageal squamous cell carcinoma. Nat Genet 2014;46:467–73. [PubMed: 24686850]
20. Buenrostro JD, Wu B, Chang HY, Greenleaf WJ. ATAC-seq: a method for assaying chromatin accessibility genome-wide. Curr Protoc Mol Biol 2015;109:2191–9.
21. Tyner JW, Yang WF, Bankhead A 3rd, Fan G, Fletcher LB, Bryant J, et al. Kinase pathway dependence in primary human leukemias determined by rapid inhibitor screening. Cancer Res 2013;73:285–96. [PubMed: 23087056]
22. Bicocca VT, Chang BH, Masouleh BK, Muschen M, Loriaux MM, Druker BJ, et al. Crosstalk between ROR1 and the Pre-B cell receptor promotes survival of t(1;19) acute lymphoblastic leukemia. Cancer Cell 2012;22:656–67. [PubMed: 23153538]
23. Chan KC, Ting CM, Chan PS, Lo MC, Lo KW, Curry JE, et al. A novel Hsp90 inhibitor AT13387 induces senescence in EBV-positive nasopharyngeal carcinoma cells and suppresses tumor formation. Mol Cancer 2013; 12:128. [PubMed: 24156782]
24. Jiang H, Fan D, Zhou G, Li X, Deng H. Phosphatidylinositol 3-kinase inhibitor(LY294002) induces apoptosis of human nasopharyngeal carcinoma in vitro and *in vivo*. J Exp Clin Cancer Res 2010;29:34. [PubMed: 20412566]
25. Hsu CH, Gao M, Chen CL, Yeh PY, Cheng AL. Inhibitors of epidermoid growth factor receptor suppress cell growth and enhance chemosensitivity of nasopharyngeal cancer cells *in vitro*. Oncology 2005;68:538–47. [PubMed: 16037687]
26. Asghar U, Witkiewicz AK, Turner NC, Knudsen ES. The history and future of targeting cyclin-dependent kinases in cancer therapy. Nat Rev Drug Discov 2015;14:130–46. [PubMed: 25633797]
27. Besson A, Dowdy SF, Roberts JM. CDK inhibitors: cell cycle regulators and beyond. Dev Cell 2008;14:159–69. [PubMed: 18267085]
28. Akhtar MS, Heidemann M, Tietjen JR, Zhang DW, Chapman RD, Eick D, et al. TFIIH kinase places bivalent marks on the carboxy-terminal domain of RNA polymerase II. Mol Cell 2009;34:387–93. [PubMed: 19450536]
29. Glover-Cutter K, Kim S, Espinosa J, Bentley DL. RNA polymerase II pauses and associates with pre-mRNA processing factors at both ends of genes. Nat Struct Mol Biol 2008;15:71–8. [PubMed: 18157150]
30. Larochelle S, Amat R, Glover-Cutter K, Sanso M, Zhang C, Allen JJ, et al. Cyclin-dependent kinase control of the initiation-to-elongation switch of RNA polymerase II. Nat Struct Mol Biol 2012;19:1108–15. [PubMed: 23064645]
31. Eilers M, Eisenman RN. Myc's broad reach. Genes Dev 2008;22:2755–66. [PubMed: 18923074]
32. Yu Y, Dong W, Li X, Yu E, Zhou X, Li S. Significance of c-Myc and Bcl-2 protein expression in nasopharyngeal carcinoma. Arch Otolaryngol Head Neck Surg 2003;129:1322–6. [PubMed: 14676159]
33. Crook T, Nicholls JM, Brooks L, O'Nions J, Allday MJ. High level expression of deltaN-p63: a mechanism for the inactivation of p53 in undifferentiated nasopharyngeal carcinoma (NPC)? Oncogene 2000;19:3439–44. [PubMed: 10918601]
34. Truong AB, Kretz M, Ridky TW, Kimmel R, Khavari PA. p63 regulates proliferation and differentiation of developmentally mature keratinocytes. Genes Dev 2006;20:3185–97. [PubMed: 17114587]

Author Manuscript Author Manuscript Author Manuscript Author Manuscript

35. Ruan L, Li XH, Wan XX, Yi H, Li C, Li MY, et al. Analysis of EGFR signaling pathway in nasopharyngeal carcinoma cells by quantitative phosphoproteomics. Proteome Sci 2011;9:35. [PubMed: 21711528]
36. Thornburg NJ, Pathmanathan R, Raab-Traub N. Activation of nuclear factor-kappaB p50 homodimer/Bcl-3 complexes in nasopharyngeal carcinoma. Cancer Res 2003;63:8293–301. [PubMed: 14678988]
37. Hirata H, Hinoda Y, Shahryari V, Deng G, Nakajima K, Tabatabai ZL, et al. Long noncoding RNA MALAT1 promotes aggressive renal cell carcinoma through Ezh2 and interacts with miR-205. Cancer Res 2015;75:1322–31. [PubMed: 25600645]
38. Chakravarty D, Sboner A, Nair SS, Giannopoulou E, Li R, Hennig S, et al. The oestrogen receptor alpha-regulated lncRNA NEAT1 is a critical modulator of prostate cancer. Nat Commun 2014;5:5383. [PubMed: 25415230]
39. Ma MZ, Chu BF, Zhang Y, Weng MZ, Qin YY, Gong W, et al. Long non-coding RNA CCAT1 promotes gallbladder cancer development via negative modulation ofmiRNA-218–5p. Cell Death Dis 2015;6:e1583. [PubMed: 25569100]
40. Klijn C, Durinck S, Stawiski EW, Haverty PM, Jiang Z, Liu H, et al. A comprehensive transcriptional portrait of human cancer cell lines. Nat Biotechnol 2015;33:306–12. [PubMed: 25485619]
41. Choudhry H, Albukhari A, Morotti M, Haider S, Moralli D, Smythies J, et al. Tumor hypoxia induces nuclear paraspeckle formation through HIF-2alpha dependent transcriptional activation of NEAT1 leading to cancer cell survival. Oncogene 2015;34:4546. [PubMed: 26289678]
42. Gutschner T, Hammerle M, Eissmann M, Hsu J, Kim Y, Hung G, et al. The non-coding RNA MALAT1 is a critical regulator of the metastasis phenotype of lung cancer cells. Cancer Res 2013;73:1180–9. [PubMed: 23243023]
43. Bradner JE, Hnisz D, Young RA. Transcriptional Addiction in Cancer. Cell 2017;168:629–43. [PubMed: 28187285]
44. Takei Y, Ishikawa S, Tokino T, Muto T, Nakamura Y. Isolation of a novel TP53 target gene from a colon cancer cell line carrying a highly regulated wild-type TP53 expression system. Genes Chromosomes Cancer 1998; 23:1–9. [PubMed: 9713990]
45. Diaz-Lagares A, Crujeiras AB, Lopez-Serra P, Soler M, Setien F, Goyal A, et al. Epigenetic inactivation of the p53-induced long noncoding RNA TP53 target 1 in human cancer. Proc Natl Acad Sci U S A 2016;113:E7535–E44. [PubMed: 27821766]
46. Seth A, Watson DK. ETS transcription factors and their emerging roles in human cancer. Eur J Cancer 2005;41:2462–78. [PubMed: 16213704]
47. Xu D, Dwyer J, Li H, Duan W, Liu JP. Ets2 maintains hTERT gene expression and breast cancer cell proliferation by interacting with c-Myc. J Biol Chem 2008;283:23567–80. [PubMed: 18586674]
48. Mosrati MA, Malmstrom A, Lysiak M, Krysztofiak A, Hallbeck M, Milos P, et al. TERT promoter mutations and polymorphisms as prognostic factors in primary glioblastoma. Oncotarget 2015;6:16663–73. [PubMed: 26143636]
49. Kabbout M, Garcia MM, Fujimoto J, Liu DD, Woods D, Chow CW, et al. ETS2 mediated tumor suppressive function and MET oncogene inhibition in human non-small cell lung cancer. Clin Cancer Res 2013;19: 3383–95. [PubMed: 23659968]
50. Luo Z, Zhang L, Li Z, Li X, Li G, Yu H, et al. An *insilico* analysis of dynamic changes in microRNA expression profiles in stepwise development of nasopharyngeal carcinoma. BMC Med Genomics 2012;5:3. [PubMed: 22260379]

Author Manuscript Author Manuscript Author Manuscript Author Manuscript

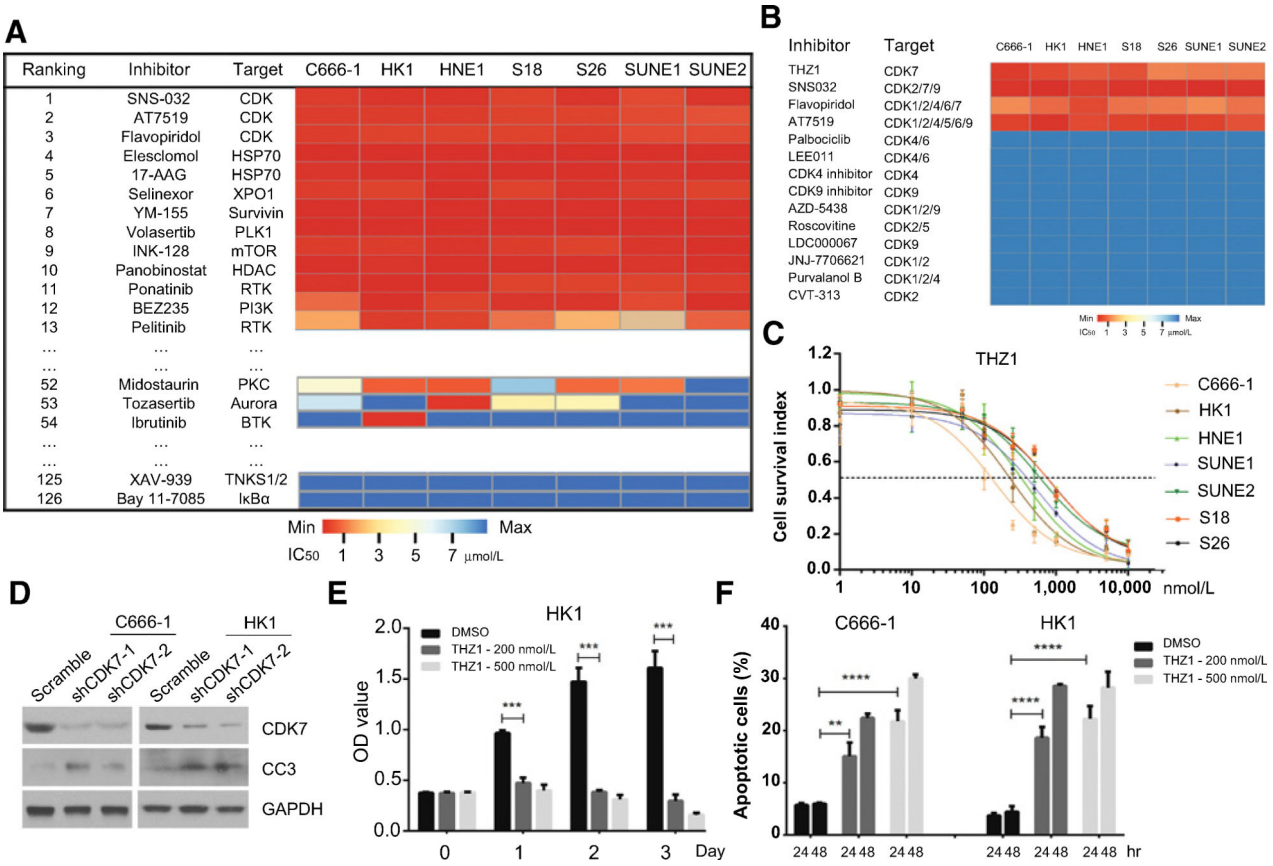

Figure 1.

High-throughput chemical screening identifies THZ1 as a potent inhibitor of NPC cells. Heatmap showing the sensitivity of seven NPC lines to 126 small-molecule chemicals in high-throughput screening (**A**; only partial list of inhibitors shown) and a panel of 14 different CDK inhibitors ranked by IC_{50} values (**B**). The entire results of **A** and **B** are presented in Supplementary Fig. S1 and Supplementary Tables S1 and S2. **C,** Cell viability assay measuring the dose response of NPC cell lines to THZ1. Data are presented as mean ± SD of three replicates. **D,** Immunoblotting analysis quantifying the expression of CDK7 and cleaved caspase-3 (CC3) upon CDK7 knockdown. GAPDH was used as a loading control. **E,** Cell viability assays showing the effects of THZ1 treatment on HK1 NPC cells at indicated time points and doses. Data are presented as mean ± SD of three replicates. ***, $P < 0.001$. **F,** Apoptosis analysis in C666-1 and HK1 cells treated with THZ1. Data are presented as mean ± SD of three replicates. **, $P < 0.01$; ****, $P < 0.0001$.

Author Manuscript Author Manuscript Author Manuscript Author Manuscript

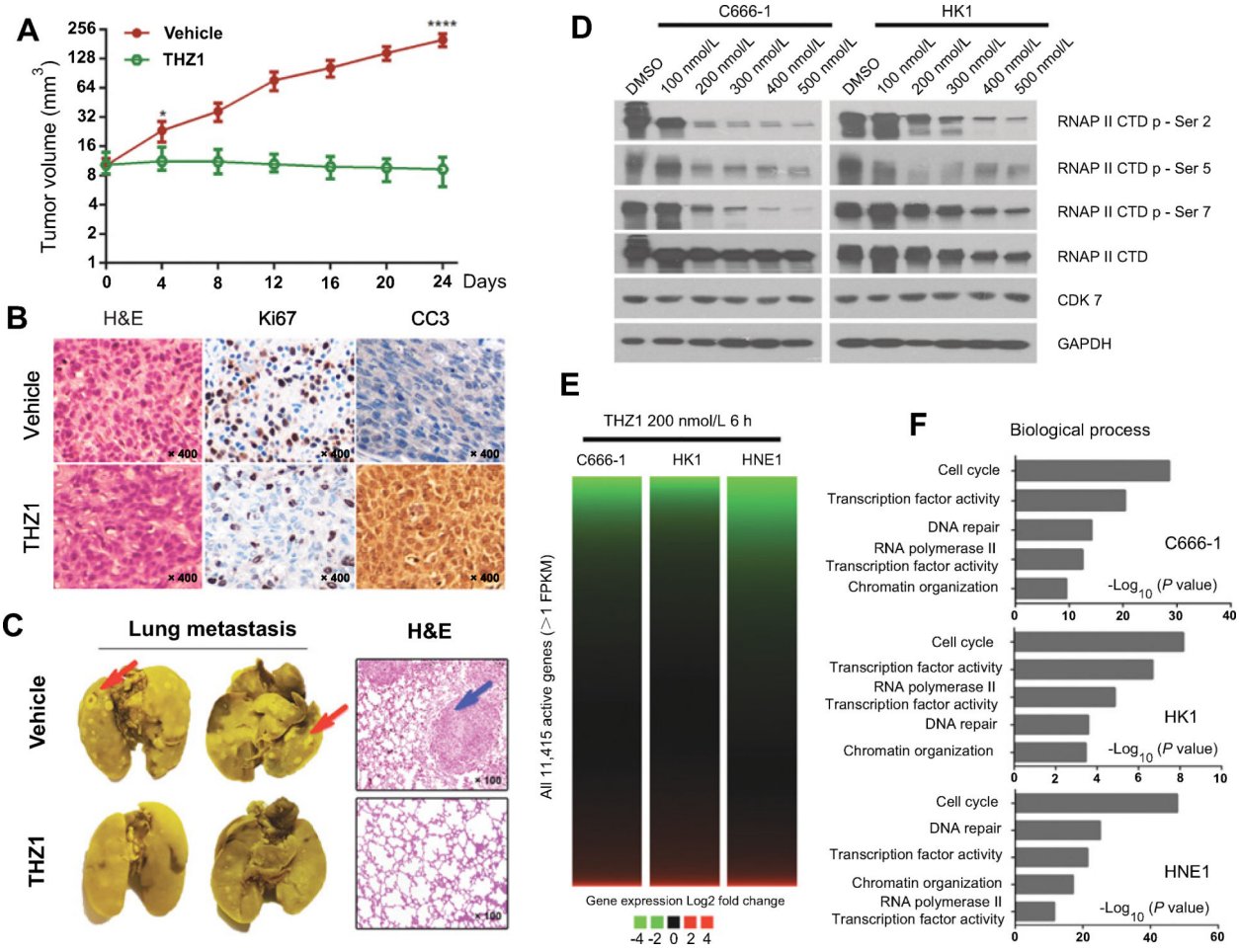

Figure 2.

THZ1: selective Inhibition of RNAPII-mediated transcription. **A,** Tumor growth curve of mice injected with either THZ1 or vehicle. Data represent mean ± SD of each group. *, $P < 0.05$; ****, $P < 0.0001$. **B,** Hematoxylin and eosin (H&E) and IHC staining of Ki67 and CC3 in tumor tissue sections. Original magnification, ×400. **C,** Metastasis model. Representative images of mouse lungs after Bouin's fixation (left) and hematoxylin and eosin staining (right). Arrows, tumor metastases nodule. **D,** Immunoblot analysis of the levels of RNAPII CTD phosphorylation in C666-1 and HK1 cells treated with either THZ1 or DMSO at indicated concentrations for 12 hours. **E,** Heatmaps of gene expression in C666-1, HK1, and HNE1 NPC cells treated with THZ1 (200 nmol/L for 6 hours) relative to DMSO group. **F,** GO enrichment analysis of THZ1-sensitive transcripts in three NPC cell lines.

Author Manuscript Author Manuscript Author Manuscript Author Manuscript

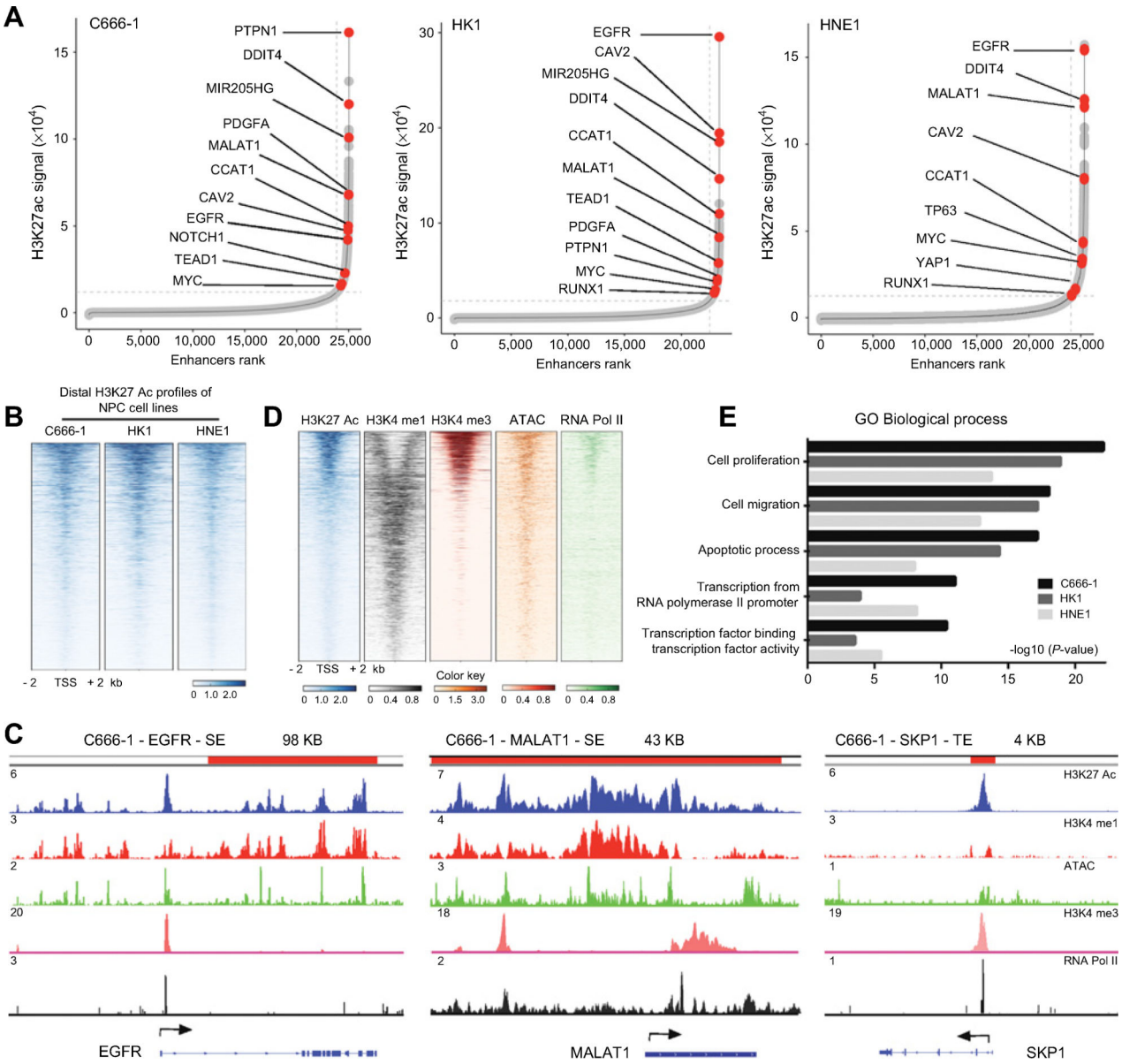

Figure 3.

Profiling of the SE landscapes in NPC cell lines. **A,** Hockey stick plots in NPC cells showing input-normalized, rank-ordered H3K27ac signals, highlighting a number of SE-associated genes. **B,** Heatmaps of ChIP-Seq signal intensity of H3K27ac [±2-kb windows around the center of transcription start site (TSS)] for three NPC cell lines, ordered by their mean signal. **C,** ChIP-seq profiles of H3K27ac, H3K4me1, H3K4me3, ATAC, and RNA Pol II binding at representative SE (EGFR and MALAT1)- or TE (SKP1)-associated gene loci in C666-1 NPC cells. **D,** Heatmaps of ChIP-seq profiles of H3K27ac, H3K4me1, H3K4me3, ATAC, and RNA Pol II, ordered by H3K27ac signal (C666-1). **E,** GO enrichment analysis of SE-associated genes.

Author Manuscript
Author Manuscript
Author Manuscript
Author Manuscript

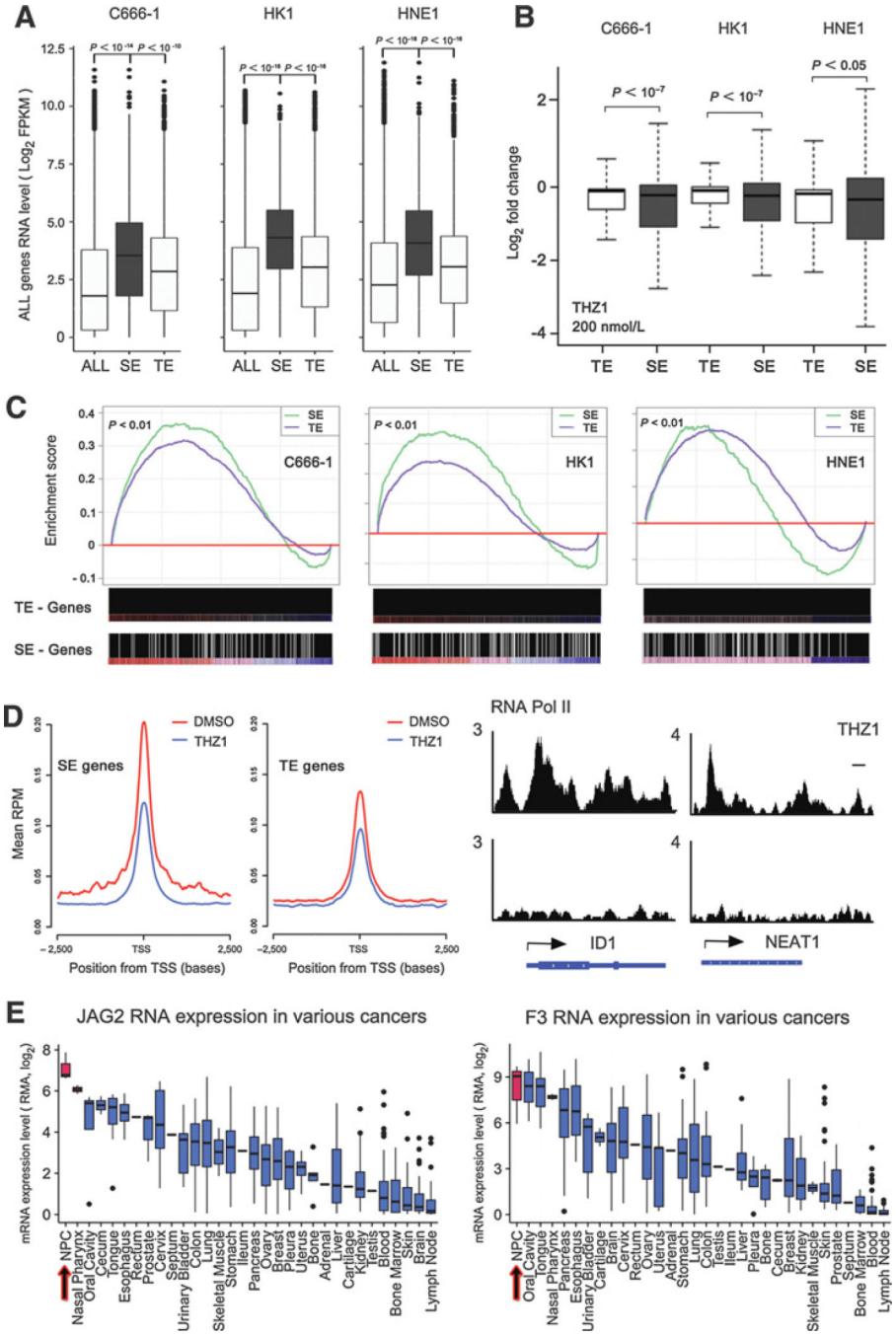

Figure 4.

Characterizing the biological features of SE-associated transcripts in NPC. **A** and **B,** Box plots showing RNA expression levels (**A**) of transcripts associated with total pool of enhancers (ALL), TEs, and SEs, as well as their fold changes upon THZ1 treatment (**B**; 6 hours). **C,** GSEA of the fold changes of either SE- or TE-associated transcripts following THZ1 treatment. **D,** Representative ChIP-seq profiles showing that RNA Pol II occupancy across promoters and gene bodies was reduced upon THZ1 treatment. **E,** mRNA expression levels of JAG2 and F3 across various types of human cancers. Data were retrieved from the

dataset E-MTAB-2706, which contains RNA-seq of 675 human cancer cell lines. Arrow, NPC cells.

Author Manuscript Author Manuscript Author Manuscript Author Manuscript

Author Manuscript Author Manuscript Author Manuscript Author Manuscript

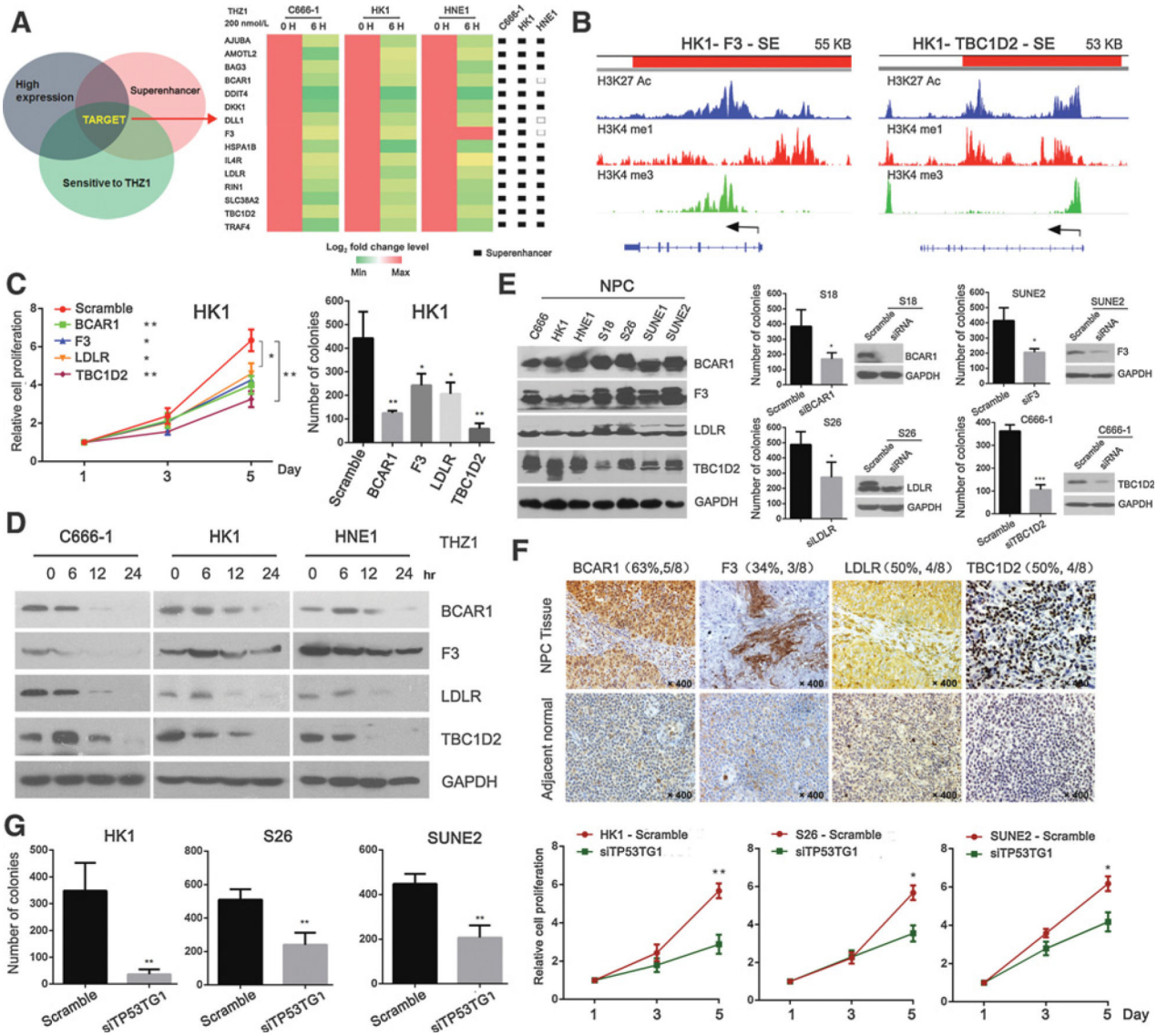

Figure 5.

Identification of novel SE-associated oncogenes in NPC. **A,** Outline of the integrative analysis to nominate novel SE-associated oncogenes in NPC. Heatmaps on the right show the expression level of candidate genes following THZ1 treatment and their SE status in each cell line. **B,** Representative H3K27ac ChIP-seq profiles of two novel candidates, F3 and TBC1D2, in HK1 cells. **C,** Cell viability and colony formation assays demonstrating that four novel SE-associated candidate oncogenes were essential for cell proliferation and clonogenic growth of HK1 cells. **D,** Immunoblotting analysis verifying that the protein levels of the four novel SE-associated oncogenes were rapidly decreased by THZ1. **E,** Immunoblotting showing the protein levels of these four candidates in seven NPC cell lines (left) and representative colony formation results of NPC cells transfected with indicated siRNAs (right). **F,** Representative IHC photos displaying the expression of four novel oncogenes in primary NPC samples and the adjacent normal tissue. **G,** Growth-suppressive effect of silencing TP53TG1 in three NPC cell lines as assayed by colony formation (left)

Author Manuscript Author Manuscript Author Manuscript Author Manuscript

and cell viability (right). Data of **C**, **E**, and **G** represent the mean ± SD ($n = 3$; *, $P < 0.05$; **, $P < 0.01$; ***, $P < 0.001$).

Author Manuscript Author Manuscript Author Manuscript Author Manuscript

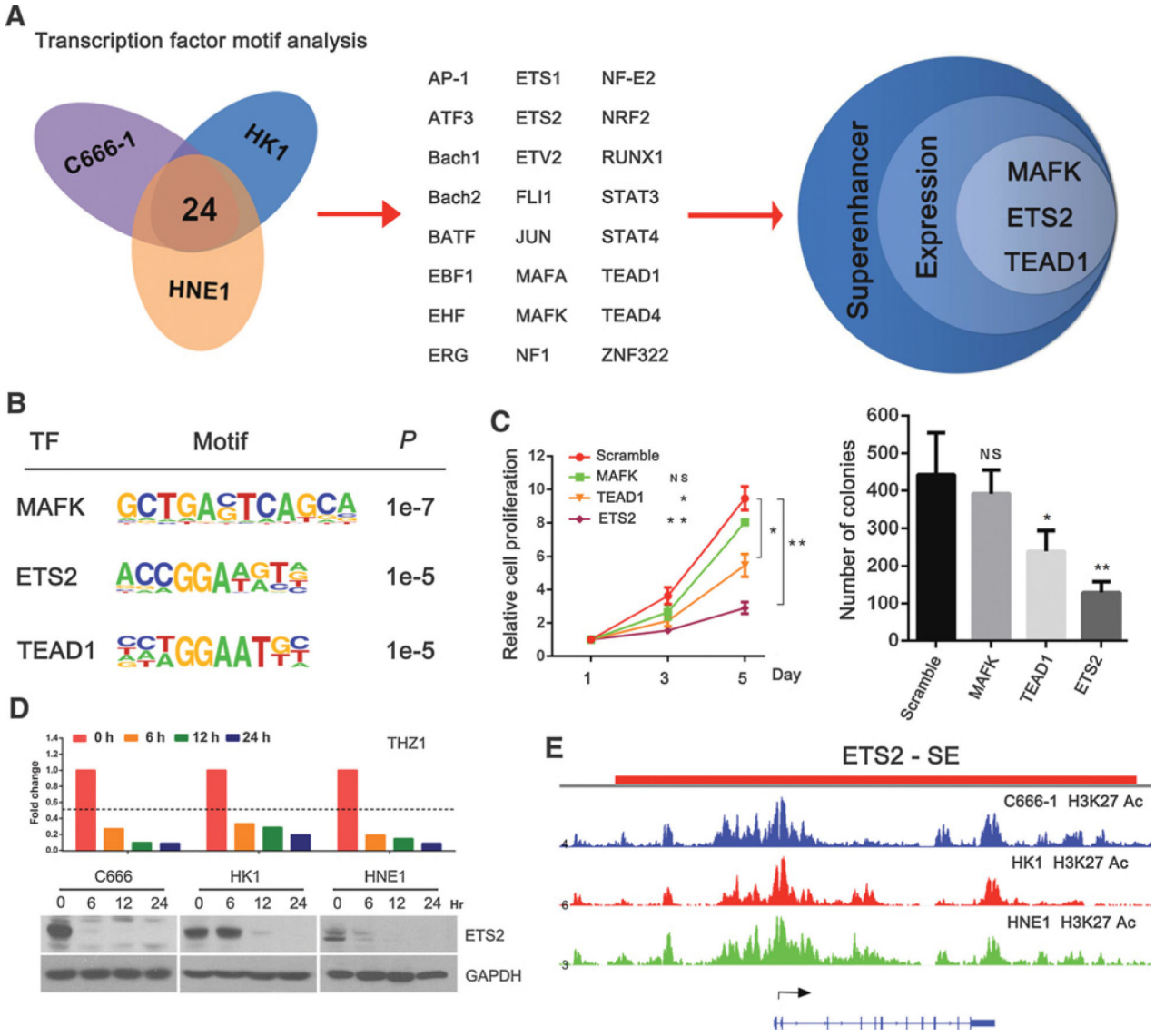

Figure 6.

Characterization of SE-associated master TFs in NPC. **A,** Strategy of identifying SE-promoting master TFs in NPC cell lines. Following *de novo* motif analysis of all SE genomic regions, master TFs were (i) associated with SE and (ii) actively expressed in all three NPC cells. **B,** TF motifs enriched at NPC super-enhancers compared with other enhancers. **C,** Cell viability and colony formation assays showing ETS2 and TEAD promoted cell proliferation (left) and clonogenic growth (right) in HK1 cells. **D,** Prominent sensitivity of ETS2 expression to THZ1 (6, 12, and 24 hours) was quantified by qRT-PCR (top) and immunoblotting (bottom). **E,** H3K27ac ChIP-seq profiles of ETS2 in C666-1, HK1, and HNE1 cells.

Author Manuscript Author Manuscript Author Manuscript Author Manuscript

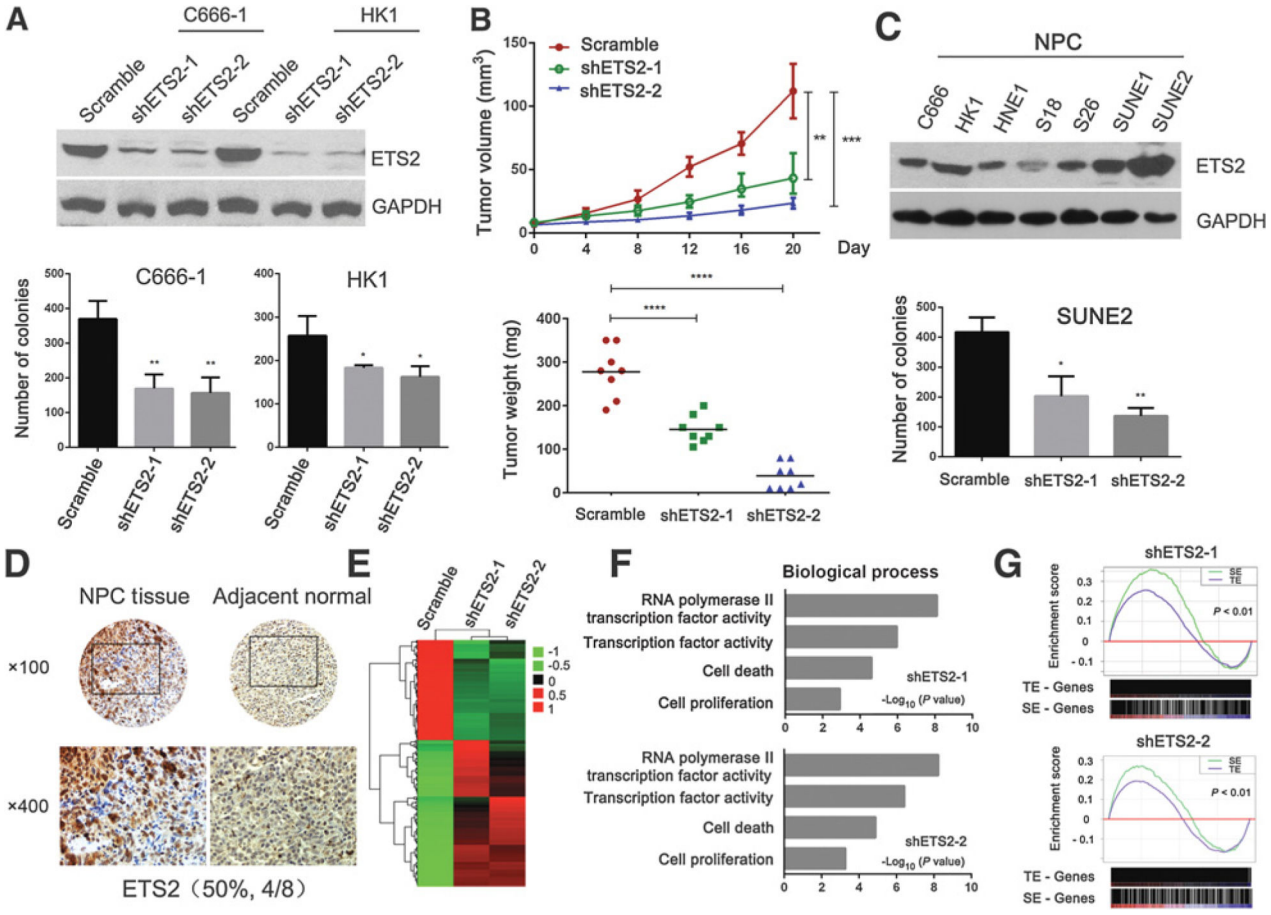

Figure 7.

Establishing ETS2 as an SE-associated master TF in NPC. **A,** ETS2 expression was silenced by two independent shRNAs as validated by immunoblotting (top). Number of NPC colonies decreased after silencing ETS2 (bottom). **B,** ETS2 knockdown potently inhibited growth of NPC xenografts in NSG mice (top); weight of tumors was calculated at the end of the experiment (bottom). **C,** Immunoblot analysis measuring ETS2 protein expression in different NPC cell lines (top); silencing ETS2 decreased colony formation of SUNE2 cells (bottom, constitutively high ETS2 level). **D,** Representative ETS2 IHC expression in NPC and normal adjacent tissue. **E,** Heatmap of the RNA-seq results following ETS2 silencing. **F,** GO enrichment analysis of downregulated genes upon ETS2 knockdown. **G,** GSEA of downregulated genes upon ETS2 silencing. Data of **A–C** represent mean ± SD ($n = 3$; *, $P < 0.05$; **, $P < 0.01$; ***, $P < 0.001$; ****, $P < 0.0001$).